# Localized Photoelectrochemistry on a Tungsten Oxide–Iron Oxide Thin Film Material Library

Jan Philipp Kollender,[†] Andrei Ionut Mardare,[†] and Achim Walter Hassel*,[†,‡]

[†]Institute for Chemical Technology of Inorganic Materials, and [‡]Christian Doppler Laboratory for Combinatorial Oxide Chemistry at Institute for Chemical Technology of Inorganic Materials, Johannes Kepler University Linz, Altenberger Strasse 69, 4040 Linz, Austria

ABSTRACT: A WO_3–Fe_2O_3 thin film combinatorial library was fabricated using a vapor phase co-deposition method followed by a combined thermal annealing and oxidation process. The scanning electron microscopy (SEM) analysis of the library microstructure combined with X-ray diffraction (XRD) investigations suggested that α-Fe_2O_3 grains preferentially grow from boundaries of domains, containing finer grains of WO_3 and Fe_2WO_6, forming filiform networks on the surface. The surface density of the hematite networks depends on the amount of Fe present in the library. Photocurrents measured at different applied biases using Photo Electrochemical Scanning Droplet Cell Microscopy (PE-SDCM) were analyzed and mapped along the entire compositional spread. A distinctive photocurrent peak was detected at 21.9 atom % Fe, and its appearance was correlated to the higher amount of hematite present in the library at this specific composition together with a specific WO_3 crystallographic orientation ((222) orthorhombic or (400) monoclinic). This finding is confirmed by qualitative and quantitative XPS surface analysis at the photocurrent peak position in the material library. Thus the enhancement of the photocurrent cannot be exclusively attributed to certain surface modifications since only hematite was found on the library surface at the peak composition.

KEYWORDS: electrocatalyst, photoanodes, water splitting, metal oxides, photo electrochemical scanning droplet cell microscopy (PE-SDCM), localized photoelectrochemistry
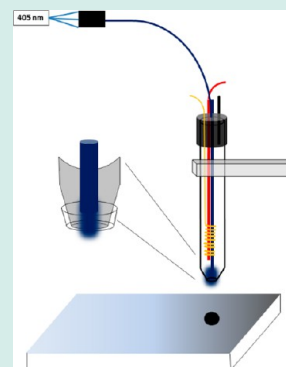
1. INTRODUCTION

The search for a stable and inexpensive photoanode being able to photoelectrolyze water using visible light has been a hot topic in photoelectrochemical research since the first oil crisis in the 1970s.[1] Both, α-Fe_2O_3 (Hematite) and WO_3 have received much attention because of their abundance, nontoxicity, and electrochemical stability.[2]

Thin films of both oxides can be prepared by various methods like sputtering, thermal evaporation, electrodeposition, spray pyrolysis, and chemical vapor deposition. Despite its rather low bandgap between 1.9 and 2.2 eV and a lot of research efforts in the past, α-Fe_2O_3 photoanodes still have a rather low efficiency because of low absorption coefficients, a high recombination rate, and a rather short charge carrier diffusion length. Additionally, the conduction band edge of hematite is too low to allow spontaneous water splitting which means that an additional applied bias is necessary for water splitting.[3] One method used to improve the performance of hematite thin films has been to incorporate other metals, such as Nb, Ti, and Si, into the hematite.[4]

WO_3 is an excellent catalyst for water oxidation and has been used in various forms as a photoanode in water-splitting systems for nearly 4 decades. It has good chemical stability in acids, good electrical transport properties, and its ability to absorb a reasonable portion of the solar spectrum makes it a promising candidate. Because of its rather large band gap of 2.7–3.1 eV, WO_3 mainly absorbs in the blue and near-ultraviolet region of the solar spectrum.[5] To increase the photocatalytic activity of WO_3 it was modified with transition metal oxides such as TiO_2 and Fe_2O_3.[6,7] Recently there has also been a combinatorial study on nanostructured WO_3 thin film photoanodes produced by dealloying of binary alloys.[8]

In this study a mixed oxide material library of WO_3 and Fe_2O_3 has been prepared using the rather inexpensive method of thermal evaporation from two different sources which covers nearly 90% of the possible compositional range. A detailed investigation of the obtained material library was done using energy dispersive X-ray spectroscopy (EDX), scanning electron microscopy (SEM), X-ray diffraction (XRD), and X-ray photoelectron spectroscopy (XPS). Photocurrents were measured locally using PE-SDCM[9] with an atomic resolution better than 0.5 atom %. Significant increases in the photocurrent were observed at certain contents of Fe_2O_3.

2. EXPERIMENTAL PROCEDURES

2.1. Thin Film Combinatorial Library Fabrication. To investigate the properties of the WO_3–Fe_2O_3 system over a wide compositional range, a WO_3–Fe thin film combinatorial library was first produced. The library was co-deposited from the vapor phase using two independent sources (WO_3 and Fe)

using an in house developed state of the art thermal co-evaporator. A maximum of three different thermal evaporation sources can be used simultaneously in a stainless steel vacuum chamber. The sources are positioned equidistantly in a circular geometry so that the center of each source lies on a circle of 100 mm (4 in.) in diameter defining the edge of a sample (e.g., Si wafer). High purity Cu rods, serving as electrical feedthroughs for providing the high currents necessary for the thermal elements, are externally attached to air-air heat exchangers with a nominal cooling power of 300 W each. The air cooling is used for thermally stabilizing the Cu rods during the evaporation process. The background vacuum level is in the range of 10^{-5} Pa ensuring a very low contaminant level during the film formation. Using crystal quartz balances (Inficon-SQM242 acquisition board), the flux of each source can be individually controlled and the desired compositional gradient can be obtained by adjusting the evaporation power through a self-made PID controller (LabView software). Moreover, each source can be individually moved in the vertical plane so that the source-substrate distance can be adjusted for each element. This action will affect the individual thickness gradients through the cosine law of evaporation, giving the user an extra degree of freedom for tuning the final library composition. For the deposition of the WO_3-Fe compositional spread, a source-substrate distance of 120 mm was used for both sources.

As substrates, 100 mm (4 in.) p-type silicon wafers (Si-Mat Silicon Materials, Landsberg am Lech, Germany) with an electrical resistivity of 10−20 Ω cm and a thickness of 525 ± 25 μm were used. The Si wafers were directly taken from a sealed box without further cleaning or processing. Iron powder of 99.99% purity (Merck KGaA, Darmstadt, Germany) was used for evaporation from a boron nitride crucible (1.5 cm^3) heated by a tungsten basket. The thermal element was connected to a DC power source (Sorensen, XG20-84) with a maximum deliverable power of 1.65 kW. As the second evaporation source, WO_3 powder of 99.9% purity (Sigma-Aldrich, Munich, Germany) was placed in a tungsten notched dimple boat (Kurt. J. Lesker). This was powered by a high current power supply (FuG-Elektronik, NLN1400-6.5) able to deliver a maximum of 780 W. To obtain the WO_3-Fe combinatorial library by simultaneously using both evaporation sources, the individual evaporation rates were tuned for maximizing the total achievable compositional gradient. Two different pairs of deposition rates were sequentially used for obtaining two different samples which together provided a wide compositional spread. Deposition rate of 1.5 nm s^{-1} for the WO_3 together with a rate of 0.01 nm s^{-1} for the Fe deposition was used for deposition on the first Si wafer. In a second deposition, 0.48 nm s^{-1} for WO_3 combined with 0.1 nm s^{-1} for Fe deposition was used to deposit a second material library with an overall higher Fe content. Both samples fabricated in this manner defined the WO_3-Fe combinatorial library investigated in this work.

To obtain the $WO_3-Fe_2O_3$ combinatorial library, a thermal heat treatment was applied to the as-deposited WO_3-Fe library.[10] This process is necessary on one hand for the reoxidation of WO_3 that tend to evaporate in its hexavalent state and condenses, at least to some extent, in subvalent states. On the other hand a conversion of Fe into Fe_2O_3 is required. For this purpose the WO_3-Fe thin films were furnace annealed in air at 773 K for 6 h using heating and cooling rates of 2 K min^{-1}. The elemental composition of the $WO_3-Fe_2O_3$ thin film combinatorial library after annealing was measured using a Zeiss 1540-XB scanning electron microscope with a built-in

EDX analyzer (INCA X-sight, Oxford Instruments). The EDX-detector was carefully calibrated prior to measurements. Analysis of measured EDX-data was performed using INCA-software. Results were derived from spectra measured with 15 kV acceleration voltage and an acquisition time of 300 s for each spot, taking into account the different element specific yields. The coordinate origin of the scanned line was defined using the corner of the Si wafer flat cut which was nearest to the Fe evaporation source. A line of spots equally distanced from each other spreading along the entire library was automatically measured. The surface microstructure and crystallographic characteristics of the $WO_3-Fe_2O_3$ combinatorial library were investigated using SEM (Zeiss 1540-XB) and XRD (Philips X'Pert Pro), respectively. A Theta Probe X-ray photoelectron spectrometer (XPS) from Thermo Fisher with Al Kα anode at energy of 1486.7 eV and a spot size of 400 μm was used to characterize the surface of the material library. The properties were mapped along the compositional gradient using the position information coming from the EDX investigations.

2.2. Photoelectrochemical Scanning Droplet Cell Microscopy. The photoelectrochemical properties of the $WO_3-Fe_2O_3$ combinatorial library were mapped as a function of the composition. All electrochemical measurements were carried out using a photoelectrochemical scanning droplet cell microscope (PE-SDCM).[9] The outer body of the cell was made from a 2.5 mm outer diameter boron-silicate glass capillary with a wall thickness of 0.65 mm. The small opening of the tip was obtained by thermally tapering the glass using a capillary puller (PC-10, Narishige, Tokyo, Japan). The final adjustment of the tip was done by using a self-developed capillary grinder with a fast rotating disk in contact with grades 1200 and 2400 SiC sandpapers (Struers A/S, Ballerup, Denmark). After grinding, a silicone gasket was formed at the rim of the capillary tip by dipping it into liquid silicone (RTV 118Q, Momentive, Albany, U.S.A.). The silicon gasket was dried in a nitrogen flow for several hours. The exact size of the wetted area was determined by optical recognition of colored titanium dioxide formed within an anodization spot on a titanium plate as previously described for hafnium.[11] The diameter of the wetted spot was found to be 193 μm. As reference electrode (RE), a μ-Ag/AgCl system was used.[12] To prepare this electrode, AgCl was deposited on a 100 μm in diameter Ag wire (99.999% Wielandt Dentaltechnik, Germany) by polarizing it in 1 M p.a. grade HCl. The Ag/AgCl wire was inserted into a 360 μm inner diameter boron silicate glass capillary which was filled with an agar-immobilized 3 M KCl electrolyte. The potential of the μ-RE was calibrated against a commercial 3.5 M Ag/AgCl and was found to be 0.221 V versus the standard hydrogen electrode (SHE). More details about the fabrication and characterization of such electrodes can be found elsewhere.[13] The counter electrode (CE) was a 100 μm in diameter Au wire (99.999% Wielandt Dentaltechnik, Germany) which was wrapped around the RE capillary for better mechanical stability. An electrical insulation between the RE and the CE was provided by the glass capillary itself into which the RE was built. The CE was inserted together with the RE into the outer body of the droplet cell. The tip of the RE was mounted in close proximity to the sample surface which defines the working electrode (WE), in this way acting similar to a Haber−Luggin capillary.

Any photoelectrochemical system needs to be able to illuminate the investigated area with a desired radiation. To achieve a homogeneous illumination of the wetted spot, a 200

μm core-diameter multimode optical fiber (Thorlabs, Munich, Germany) was installed inside the outer glass capillary of the SDCM. The optical fiber was installed in the center of the outer capillary to ensure a uniform irradiation of the working electrode. A 500 μm diameter stainless steel syringe needle was used as electrolyte inlet. Two component epoxy glue was applied to seal the top part of the outer body glass capillary and to mechanically fix all the components. As an external light source, a 405 nm laser diode (Roithner Lasertechnik, Vienna, Austria) with an optical output power of 6 mW was employed. The laser beam was coupled into the optical fiber using a self-developed optical fiber port. To measure the optical power density directly on the wetted area, a fully assembled PE-SDCM was placed on the detector surface of an optical power meter (Coherent Lasermate Q, VL54). The measured power density was 96 mW cm^{-2}. A schematic drawing of the cell used in this study is presented in Figure 1. All electrochemical measurements were carried out in a 0.1 M Na_2SO_4 electrolyte.[14]
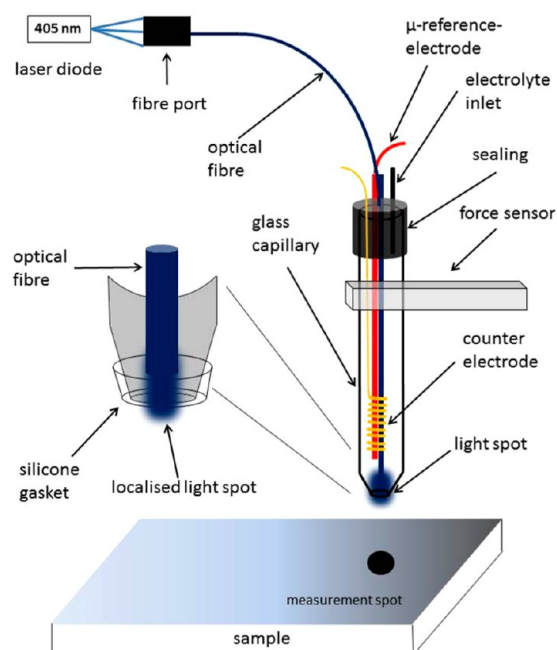

Figure 1. Schematic drawing of the Photo Electrochemical Scanning Droplet Cell Microscope (PE-SDCM)[9]

A Gantry robot, built using three linear translation stages with 150 mm travel range each, was used to position the droplet cell on the sample surface. The soft silicone sealing formed at the tip of the SDCM is used for confining the electrolyte within the inner volume of the capillary. In this way, the SDCM will operate in the contact mode, and the reproducibility of the wetted area from one addressed point to the next can be ensured to precisely control the vertical force used.[11] Only a pure elastic deformation of the silicone is desired for achieving high reproducibility. To apply a predefined force of 50 mN on each measurement spot, a force sensor was used. The complete setup was controlled by an in-house coded LabView program.

All electrochemical measurements were carried out using a CompactStat Potentiostat (Ivium Technologies, Eindhoven, The Netherlands). Current transients were carried out on each spot for 30 s to measure photocurrents at different applied

potentials. The potential was varied in 100 mV steps between 0.8 V (SHE) and 1.5 V (SHE).

3. RESULTS AND DISCUSSION

3.1. Microstructure Analysis of the WO_3–Fe_2O_3 Library.
Before the photoelectrochemical investigations on the WO_3–Fe_2O_3 thin film combinatorial library, a complete compositional and microstructural characterization was performed to investigate the properties of various oxides compounds. The compositional spread across the WO_3–Fe_2O_3 library was determined using scanning EDX analysis. Because of the large number of investigated spots, a compositional resolution better than 1 atom % was achieved. In Figure 2 the EDX results are plotted, and the detected amounts of W, Fe, and O are mapped in a complementary manner along the entire library.
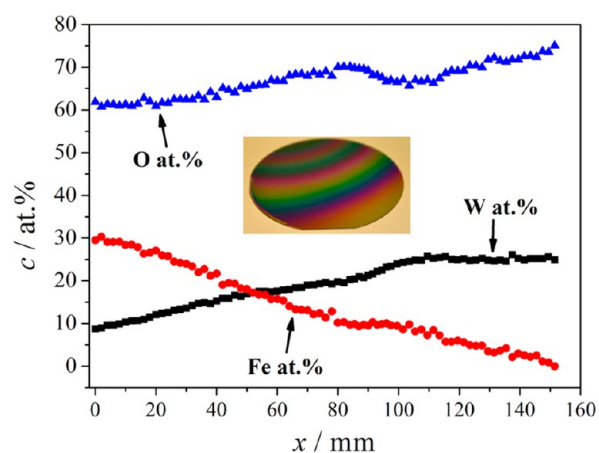

Figure 2. Compositional spread along the complete WO_3–Fe_2O_3 material library.

Starting from the point of origin (x = 0 mm), an almost linear W distribution can be observed with values ranging between 8 atom % and 25 atom % as measured at x = 90 mm. From this point, for the remaining 50 mm of the compositional spread the amount of W detected in the library was almost constant. The behavior of the Fe composition followed a similar path. At x = 0 mm the highest Fe concentration of 30 atom % was detected, and it was decreasing in a linear manner down to a value close to 0 atom % at the other extreme of the WO_3–Fe_2O_3 combinatorial library. The behavior of the O composition resembled the W compositional evolution along the library. An increase in the amount of O detected in the compositional spread ranging approximately from 60 atom % to 85 atom % was identified.

The amount of W slowly increases from one (left) side of the library to the other (right). The increase of the O content along the WO_3–Fe_2O_3 was expected to appear because of the stoichiometry differences between the two oxides. In WO_3 the metal has a higher number of corresponding O atoms as compared with Fe_2O_3, leading to an overall increase in the O content of the WO_3–Fe_2O_3 combinatorial library. A visual inspection of both wafers used in this study showed no significant differences between them. The inset of Figure 2 shows an optical photograph of one of the samples. The EDX scanned line can be easily imagined, starting at the flat-cut (x = 0) and following the clearly visible compositional gradient.
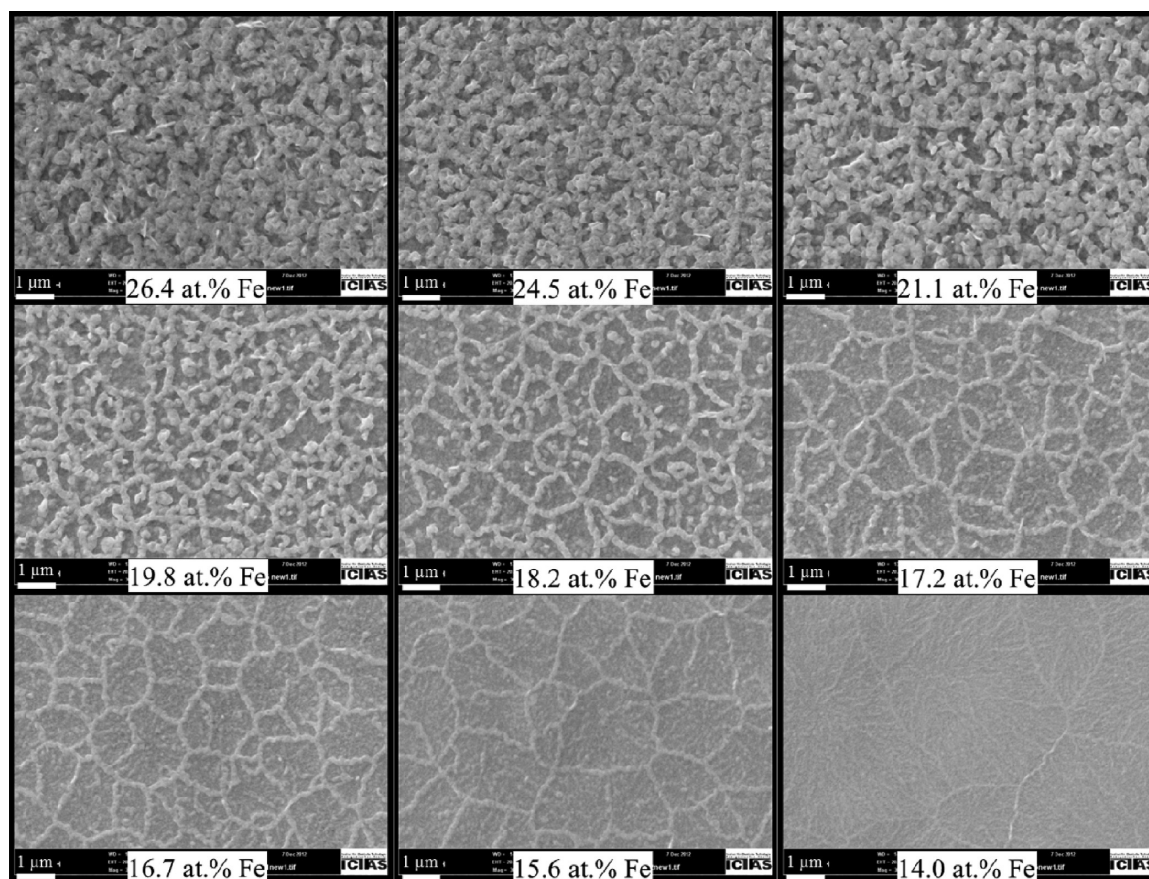
Figure 3. SEM images of the $WO_3-Fe_2O_3$ combinatorial library at different concentrations.

The surface microstructure of the $WO_3-Fe_2O_3$ combinatorial library was analyzed using SEM to study the gradual surface effects of the mixture of both oxides at various ratios. In Figure 3 several such images are presented for selected compositions along the entire library.

At high concentration of Fe (26.4 atom %), a specific surface microstructure can be observed. The surface is almost completely covered by grains with sizes of approximately 300 nm connected to each other. The connection established between adjacent grains resulted in the formation of filament-like structures closely resembling surface features such as those encountered in filiform corrosion. With respect to this similarity the term filiform is used in the following as a descriptive term. These patterned chained grains, forming a compact filiform network on the surface, are a direct result of the thin film formation depending on the local composition of the material library. As the amount of Fe is decreased along the compositional spread, the filiform network starts to withdraw revealing the underlying surface. The confinement of the filiform network defines structural domains which became totally clear starting with 18.2 atom % Fe when first the surface of the underlying structure is exposed and can be better observed. A high number of finer grains can be observed grouped in domains most likely sharing similar microstructural properties. Imaging at higher SEM magnifications has revealed grains of approximately 100 nm in diameter forming the underlying structure of the entire compositional spread. Their size slowly decreases with the amount of Fe. The larger grains forming the network nucleate at the domain boundaries forming the previously observed filiform structure even at Fe

concentrations as low as 16.7 atom %. Decreasing even more the Fe concentration results in changes of the surface microstructure according to the decrease of the filiform network length. At the same time the size of the individual grains forming the network decreases with the amount of Fe. At low Fe contents (14 atom %) the surface of the $WO_3-Fe_2O_3$ library looks smoother with less visible domains and domain boundaries. At this low Fe concentration fine stripes can still be observed along much larger domains, the size of the grains forming them being similar to the ones forming the underlying structure. Further decreasing the amount of Fe present in the library did not affect the microstructure for values below 14 atom % Fe.

To correlate the surface microstructure with the crystallographic properties of the $WO_3-Fe_2O_3$ thin film combinatorial library, XRD investigations were done at various compositions along the compositional spread. A few relevant XRD patterns are presented in Figure 4.

Because of the very close positions of the peaks in the WO_3 system, no clear symmetry identification was possible. This problem is more accentuated at low angles where the orthorhombic and monoclinic symmetries have three overlapping peaks for 2θ angles between 23 and 25°. Nevertheless, the presence of WO_3 was clearly observed along the entire library. Hematite was also identified in the $WO_3-Fe_2O_3$ compositional spread as α-Fe_2O_3 with a higher precision as compared to WO_3. However, also in this case the low angle peaks have a higher uncertainty since the position of the α-Fe_2O_3 peak and the γ-Fe_2O_3 peak are overlapping at around 24°. The conclusion that the hematite is the oxide that is most
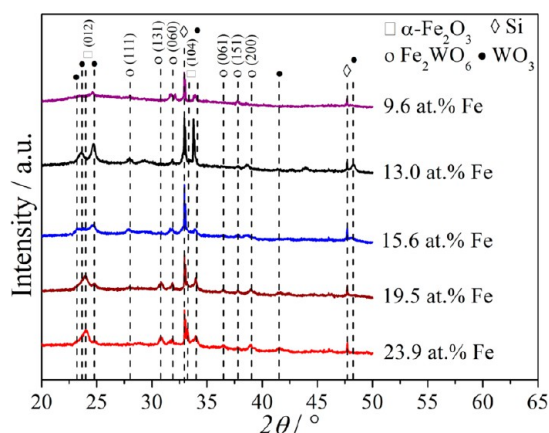
Figure 4. XRD spectra measured at various concentrations of the WO₃–Fe₂O₃ library.

likely present is supported by the position of the other α-Fe₂O₃ peaks. In addition to WO₃ and α-Fe₂O₃, the presence of Fe₂WO₆ was found in the XRD investigations describing the intimate mixing of the two oxides forming a compound along the entire library.

For very low Fe concentrations, XRD spectra very similar to the one presented for 9.6 atom % Fe were measured. The presence of a low angle WO₃ peak can be observed around 25° together with several peaks attributed to the compound Fe₂WO₆ while a clear indication of the Fe₂O₃ is missing. The situation does not change substantially with the increase of the Fe amount up to 13 atom %. While the low angle peaks of WO₃ become more pronounced and the (111), (060), (151), and (200) peaks of Fe₂WO₆ are distinguishable, the α-Fe₂O₃ still cannot be clearly identified. This result correlates to the SEM microstructure, and at this point it can be concluded that the presence of the larger grains arranged in filiform networks is related to the amount of α-Fe₂O₃. It can be suggested that the entire microstructure of the WO₃–Fe₂O₃ library is defined by WO₃/Fe₂WO₆ fine grains forming domains, while α-Fe₂O₃ nucleates from the domain boundaries forming the filiform network structure. As soon as the hematite structure forms at Fe concentrations above 15 atom %, as shown by the SEM images from Figure 3, the presence of the α-Fe₂O₃ (012) peak is suggested by the broadening of the first low angle XRD peak measured for 15.6 atom % Fe. For this concentration, the presence of the Fe₂WO₆ can be observed with the same diffraction peaks as presented earlier for 13 atom % Fe. Additionally, the WO₃ peak previously seen around 34° has a much lower intensity. At various Fe concentrations above 19 atom %, the XRD spectra showed very similar features. In Figure 4 the spectra measured at 19.5 and 23.9 atom % are also presented. A clear change in the low angle multipeak is distinctly observable in both curves. The main peak is now matching the position of (012) α-Fe₂O₃ while the WO₃ peak from around 25° decreases in height and the 48° WO₃ peak disappears. A new WO₃ peak starts to become visible at around 41.5° which was not encountered at lower Fe contents. This belongs to either the (222) orientation in the orthorhombic symmetry or the (400) orientation in the monoclinic symmetry. The (104) α-Fe₂O₃ peak starts to be better observable, first as a small shoulder of the main Si peak at 19.5 atom % Fe which is increasing its intensity for 23.9 atom % Fe. Again, this behavior leads to the same remark suggested before, that the hematite plays an important role in the

microstructural and crystallographic evolution of the WO₃– Fe₂O₃ and manifests itself through the filiform structures observed in the SEM images. Above 19 atom % Fe the increased hematite presence coincides with the disappearance of the Fe₂WO₆ (111) peak while the weak (131) and (061) already present for 15.6 atom % Fe gain in intensity.

3.2. PE-SDCM on the WO₃–Fe₂O₃ Library. To investigate the photoelectrochemical properties of the WO₃– Fe₂O₃ library, a PE-SDCM employing a 405 nm laser diode was used. Both oxides present in the library are n-type semiconductors, with the lower level of the conduction band positioned almost at the same energy of approximately −4.8 eV which is the equivalent of 0.36 V (SHE) on the electrochemical scale.[15] The bandgap reported for WO₃ has an average value of 2.9 eV while the Fe₂O₃ has a bandgap of 1.9 eV.[1] Using a simple linear approximation based on the mixed matter theory, the expected value of the oxide bandgaps in the WO₃–Fe₂O₃ library would be around 2.4 eV. The laser wavelength used in this work corresponds to an energy of 3.1 eV which matches the expected bandgaps to maximize the photocurrents. An automated scan along the compositional gradient combined with a contact mode operation allowed the irradiation of various spots and the measurement of the photocurrents for different applied anodic biases. Such measurements were done along the entire compositional spread with a compositional resolution better than 0.5 atom %. In Figure 5 a few selected photocurrent transients are presented as measured at 8 different biases ranging from 0.8 to 1.5 V.
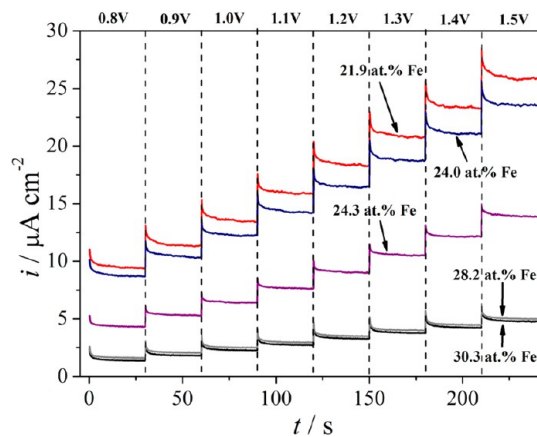

Figure 5. Selected transients of photocurrent at selected positions of the WO₃–Fe₂O₃ material library.

After each step of potential increase, an acquisition time of 30 s was sufficient for stabilizing the photocurrent into a plateau. The current overshoot observed at the beginning of each potential step describes the initial phase of additionally generated electron−hole pairs. In all curves presented in Figure 5, the clear effect of the electric field increase at the beginning of each step can be observed through the presence of increasing photocurrent plateaus. Each potential step shifts the Fermi level downward allowing a stronger hole transfer via the semiconductor-electrolyte interface as described by the anodic current levels measured. The current difference between two adjacent plateaus recorded at a specific location varies as a function of the WO₃–Fe₂O₃ library composition. At Fe concentrations above 28 atom % the current step values for the same composition and consecutive biases are below 1 µA

cm^{-2} while the absolute photocurrents measured at the same bias but different compositions are almost identical. Decreasing the Fe concentrations from 28 atom % down to 21.9 atom %, a dramatic increase of both step currents and absolute photocurrent values can be observed. Inside this compositional range the step currents increase up to 2.5 μA cm^{-2} as measured for 21.9 atom % Fe. A remarkably sharp increase of the absolute photocurrent (up to 9.7 μA cm^{-2}) can be seen when the Fe content decreases from 24.3 down to 24.0 atom %. The maximum photocurrent identified in the entire WO$_3$–Fe$_2$O$_3$ library can be found at 21.9 atom % Fe, reaching values as high as 25.9 μA cm^{-2} for the maximum applied bias of 1.5 V. Decreasing even more the Fe composition, the photocurrents start to drop, first to a level of approximately 6 μA cm^{-2} in a compositional range from 20 to 13 atom % Fe followed by levels close to zero at compositions below 13 atom % Fe (curves not shown in Figure 5).

In Figure 6 the value of the photocurrent plateaus of the selected transients (presented in Figure 5) are plotted as a
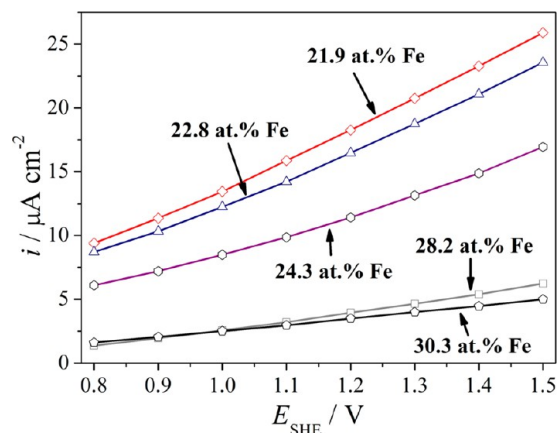

Figure 7. Measured photocurrents along the complete WO$_3$–Fe$_2$O$_3$ material library.

Figure 6. "Pseudo" linear sweeps calculated from photocurrent transients at selected Fe-concentrations.

function of the applied bias. This presentation is called "pseudo" linear sweep not because it appears almost linear but because it is usually directly measured during a linear voltage increase.

All plateau values were determined as the average of the photocurrents measured in the last 3 s for each potential step. This results in a pseudolinear sweep plot and describes the photocurrent response to the applied bias for each particular composition. The almost linear relationship between photocurrent and applied bias over the complete bias range for all selected transients suggests a constant step current value for a given composition, as it can be expected from a closer analysis of Figure 5. The increase of the positive slopes of the curves presented in Figure 6 as a function of the Fe concentration decrease, directly describes the step current evolution along the WO$_3$–Fe$_2$O$_3$ thin film library. The clear composition dependence of the absolute photocurrent increase can also be observed from the behavior of each pseudolinear sweep.

The photocurrent levels measured in the entire WO$_3$–Fe$_2$O$_3$ library are presented in Figure 7 as a compositional mapping.

Each photocurrent was measured as previously described for Figure 6, and in this case all experimental points coming from the entire compositional spread were included. Photocurrents measured at each applied bias are plotted as individual lines. Since all the photocurrent mappings share the same features in
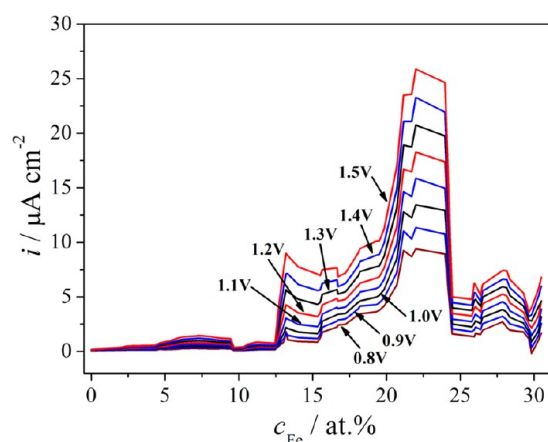
respect to the bias, all photocurrent values given in the following discussion are referred to the highest applied bias of 1.5 V$_{SHE}$ which produced the highest effect upon irradiation. Starting from the highest Fe concentration ranging down to about 25.9 atom % Fe a minimum in the photocurrent can be observed for 29.8 atom % Fe and interestingly two relative maxima were found at 27.9 and 26.0 atom % Fe. The observed photocurrent minimum has a value of approximately 3.6 μA cm^{-2} while the two local maxima show photocurrents of 7.4 and 6.2 μA cm^{-2}, respectively. In the concentration range between 25.9 and 24.5 atom % Fe the measured photocurrent is nearly constant at about 4.9 μA cm^{-2}. Decreasing the Fe content further, in the next concentration range down to 21.9 atom % Fe a remarkable increase in the photocurrent up to 25.9 μA cm^{-2} is observed, suggesting a decrease in Fe content of about 2.5 atom % that results in a five times higher photocurrent. This photocurrent of 25.9 μA cm^{-2} represents the absolute maximum photocurrent for the entire WO$_3$–Fe$_2$O$_3$ library. From this point on down to a concentration of 15.5 atom % Fe the photocurrent drops dramatically down to 6.9 μA cm^{-2}. When the Fe content further drops to 13.2 atom % a linear increase in photocurrent to 9 μA cm^{-2} is observed, representing a new local maximum of the photocurrent. As soon as the Fe content of the WO$_3$–Fe$_2$O$_3$ library drops under 13 atom %, the photocurrent sharply decreases to values as low as 0.75 μA cm^{-2} (at 12.5 atom % Fe). This total decrease in the photocurrent correlates with the complete disappearance of the filiform network on the library surface as revealed by the SEM mappings in Figure 3. Moreover, the first appearance of hematite together with the (131) and (061) peaks from the Fe$_2$WO$_6$ compound (as identified in the XRD from Figure 4 at Fe concentrations above 15.6 atom %), can be now correlated to the almost constant photocurrent measured in the compositional range of 13 to 19.5 atom %. As soon as the additional WO$_3$ peak (present at 41.5° in the XRD mapping from Figure 4) appears at 19.5 atom % Fe, the highest photocurrent peak fully develops for Fe contents up to 24.5 atom %. This indicates a clear contribution of both hematite and WO$_3$ (41.5° peak) together with the W–Fe–O compound to the enhancement of the photobehavior in this particular concentration range. For the remaining low Fe content part of the WO$_3$–Fe$_2$O$_3$ library (below 12.5 atom % Fe), the photocurrent stays very low and drops finally to nearly zero
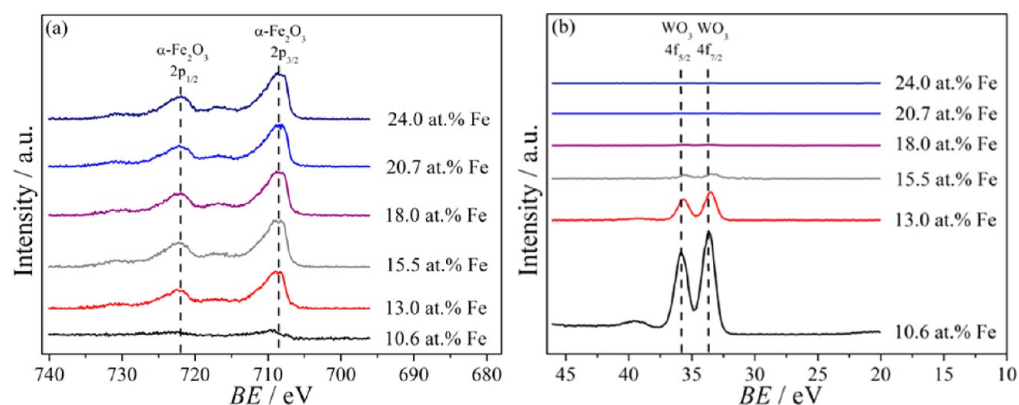
Figure 8. XPS spectra at different positions of the WO_3–Fe_2O_3 material library.

as the Fe amount decreases. A local photocurrent maximum is observed at 7.3 atom % Fe measuring only 1.47 μA cm^{-2}.

3.3. Surface Investigations of the WO_3–Fe_2O_3 Library. In an attempt to better describe and understand the surface of the WO_3–Fe_2O_3 thin film library, X-ray photoelectron spectroscopy (XPS) was used for surface analysis at various locations along the compositional spread. Using the photocurrent mapping of the entire library presented in Figure.7, the WO_3–Fe_2O_3 compositional spread was analyzed at 6 relevant compositions. One location in the low photocurrent region at 10.6 atom % Fe, three locations along the photocurrent plateau ranging between 13 and 21 atom % Fe, and two locations corresponding to the beginning (20.7 atom % Fe) and the end (24 atom % Fe) of the highest photocurrent peak.

In part (a) of Figure 8 the XPS analysis at various locations on the library (scanning XPS: SXPS) are presented as measured for the α-Fe_2O_3. For all analyzed compositions, the presence of the doublet $2p_{1/2}$-$2p_{3/2}$ was identified on the surface, with no significant peak shifts.[16] Although at low Fe concentrations the XRD investigations (9.6 atom % Fe in Figure 3) could not detect any hematite, the presence of α-Fe_2O_3 on the surface is visible at 10.6 atom % Fe. However, even though it was suggested that the enhancement of the photocurrents may be triggered by the hematite presence, the electrochemical investigations are not only limited to the exposed surface, the electron–hole pairs being also generated in the depths of the oxide. For the same compositions chosen in part (a) of Figure 8 the XPS analysis was done also for the range of binding energies corresponding to the W^{6+}. The behavior of the WO_3 on the library surface can be followed in part (b) of Figure 8. At low Fe concentrations, the WO_3 is strongly present on the surface. The position of the $4f_{5/2}$-$4f_{7/2}$ doublet is nearly constant within the experimental error of the used XPS system when the Fe concentration is increasing.[17] One may interpret the slight observed shift by 0.2 eV as a partial reduction of the WO_3 with increasing amount of Fe, but the results probably do not provide full experimental evidence for this hypothesis. The highest Fe concentration where the WO_3 is found to be present on the surface correlates with the lowest Fe concentration found during the XRD investigations where the first appearance of the hematite was observed at 15.6 atom % Fe (Figure 3). As soon as this hematite threshold is overcome at higher Fe concentrations the WO_3 could not be found on the surface, as shown by the last three spectra from part (b) of Figure 8. Since the WO_3 can still be clearly detected in the XRD spectra (Figure 3) one may conclude that the hematite preferentially segregates at the surface of the WO_3–Fe_2O_3 thin film library

while the WO_3 can be found deeper inside the mixed oxides. Both compositions defining the main photocurrent peak (Figure 7), 20.7 and 24.0 atom % Fe show a complete absence of the WO_3 from the surface, while a new XRD peak (41.5°) together with the hematite and the Fe_2WO_6 compound was observed in Figure 4. This suggests that the changes responsible for the enhancement of the photocurrent in the WO_3–Fe_2O_3 compositional spread are not superficial but rather occur deeper within the mixed oxide film.

SXPS analysis was locally done along the entire WO_3–Fe_2O_3 thin film library to quantify the detected amounts of W and Fe by integrating each individual spectrum. Such a surface composition scan is presented in Figure 9 as a surface mapping plotted against the bulk Fe concentration (given by EDX).
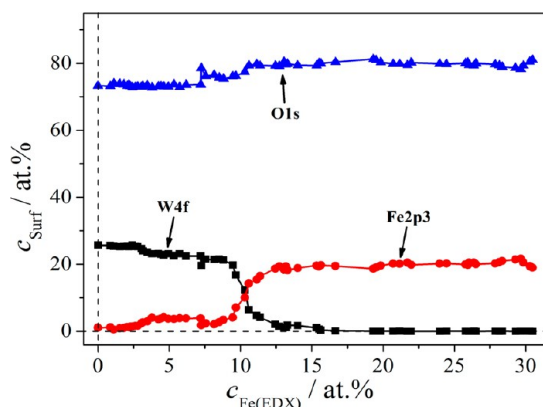

Figure 9. Elemental composition along the complete WO_3–Fe_2O_3 measured by SXPS.

The amount of oxygen found also ranges from 73 atom % at the lower bulk Fe concentration to 80 atom % at the higher bulk Fe concentration. Starting at low bulk Fe contents in the WO_3–Fe_2O_3 thin film library, only WO_3 was detected on the surface. For bulk concentrations up to approximately 3 atom % Fe the amount of Fe detected on the surface was close to zero. The stoichiometry of the WO_3 can be easily recognized by the approximately 25 atom % of W and 75 atom % of O. With the increase of the bulk Fe concentration up to 9 atom %, the hematite starts to be detected on the surface (through a maximum of 5 atom % Fe) together with the WO_3 while the photocurrents measured in Figure 7 remain low. Between 9 and 13 atom % Fe in the bulk composition, the surface undergoes a clear transition from the WO_3 to hematite. This is also visible in

the XPS spectra presented in Figure 8 and can be correlated to the transition region toward the first photocurrent peak observed above 13 atom % Fe (Figure 7). As soon as the surface is enriched with α-Fe_2O_3 and completely depleted of WO_3, the first photocurrent plateau can be identified at bulk compositions up to approximately 18 atom % Fe. At higher Fe contents, where the main photocurrent peak manifests, the surface composition does not change significantly, approximately 20 atom % Fe being detected together with 80 atom % O and almost no W which directly indicates the correct stoichiometry of α-Fe_2O_3. Also in this case, the surface compositional conservation along the photocurrent peak suggests that the factors enhancing the photocurrent in the WO_3-Fe_2O_3 library are not surface related.

4. CONCLUSIONS

In the present work, a wide range WO_3-Fe_2O_3 combinatorial thin film library was fabricated using a thermal co-evaporation technique followed by a thermal annealing for the full oxide conversion. The analysis of the library microstructure revealed a surface dynamic based on two different types of surface grains. Further XRD investigations suggested that hematite grains preferentially grow from boundaries of domains containing finer grains (most likely WO_3 and Fe_2WO_6) forming filiform networks on the surface. Photocurrents measured using PE-SDCM were analyzed and mapped along the entire compositional spread. A major and very pronounced photocurrent peak was identified at 21.9 atom % Fe, and its appearance was correlated to the higher amount of hematite present in the library at this specific composition together with WO_3 having a crystallographic orientation as either (222) orthorhombic or (400) monoclinic. XPS surface analysis allowed concluding that the photocurrent enhancement cannot be exclusively attributed to certain surface modifications, factors related more to the bulk of the oxide film needed to be considered.

■ AUTHOR INFORMATION

Corresponding Author

*E-mail: achimwalter.hassel@jku.at.

Notes

The authors declare no competing financial interest.

■ ACKNOWLEDGMENTS

■ REFERENCES

(1) Kudo, A.; Miseki, Y. Heterogeneous photocatalyst materials for water splitting. *Chem. Soc. Rev.* **2009**, *38*, 253−278.

(2) Alexander, B. D.; Kulesza, P. J.; Rutkowska, I.; Solarska, R.; Augustynski, J. J. Metal oxide photoanodes for solar hydrogen production. *Mater. Chem.* **2008**, *18*, 2298−2303.

(3) Kennedy, J. H.; Frese, K. W. Photooxidation of water at α-Fe_2O_3 Electrodes. *J. Electrochem. Soc.* **1978**, *125*, 709−714.

(4) (a) Miyake, H.; Kozuka, H. Photoelectrochemical properties of Fe_2O_3-Nb_2O_5 films prepared by Sol-Gel Method. *J. Phys. Chem. B.* **2005**, *109*, 17951−17956. (b) Kumari, S.; Singh, A. P.; Sonal; Deva, D.; Shrivastav, R.; Dass, S.; Satsangi, V. R. Spray pyrolytically

deposited nanoporous Ti^{4+} doped hematite thin films for efficient photoelectrochemical splitting of water. *Int. J. Hydrogen Energy* **2010**, *35*, 3985−3990. (c) Cesar, I.; Kay, A.; Martinez, J. A.; Grätzel, M. Translucent thin film Fe_2O_3 photoanodes for efficient water splitting by sunlight: Nanostructure-directing effect of Si-doping. *J. Am. Chem. Soc.* **2006**, *128*, 4582−4583.

(5) Janáky, C.; Rajeshwar, K.; de Tacconi, N. R.; Chanmanee, W.; Huda, M. N. Tungsten-based oxide semiconductors for solar hydrogen generartion. *Catal. Today* **2013**, *199*, 53−64.

(6) Abadias, G.; Gago, A. S.; Alonso-Vante, N. Structural and photoelectrochemical properties of $Ti_{1-x}W_xO_2$ thin films deposited by magnetron sputtering. *Surf. Coat. Technol.* **2011**, *205*, 265−270.

(7) Sivula, K.; Le Formal, F.; Grätzel, M. WO_3-Fe_2O_3 Photoanodes for Water Splitting: A Host Scaffold, Guest Absorber Approach. *Chem. Mater.* **2009**, *21*, 2862−2867.

(8) Stepanovich, A.; Sliozberg, K.; Schuhmann, W.; Ludwig, A. Combinatorial development of nanoporous WO_3 thin film photoelectrodes for solar water splitting by dealloying of binary alloys. *Int. J. Hydrogen Energy* **2012**, *37*, 11618−11624.

(9) Kollender, J. P.; Mardare, A. I.; Hassel, A. W. Photoelectrochemical Scanning Droplet Cell Microscopy (PE-SDCM). *ChemPhysChem* **2013**, *14*, 560−567.

(10) (a) Joraid, A. A.; Alamri, S. N. Effect of annealing on structural and optical properties of WO_3 thin films prepared by electron-beam coating. *Phys. B* **2007**, *391*, 199−205. (b) Moshfegh, A. Z.; Azimirad, R.; Akhavan, O. Optical properties and surface morphology of evaporated $(WO_3)_{1-x}$-$(Fe_2O_3)_x$ thin films. *Thin Solid Films* **2005**, *484*, 124−131.

(11) Mardare, A. I.; Hassel, A. W. Quantitative optical recognition of highly reproducible ultrathin oxide films in microelectrochemical anodization. *Rev. Sci. Instrum.* **2009**, *80*, 46106.

(12) Hassel, A. W.; Fushimi, K.; Seo, M. An agar-based silver vertical bar silver chloride reference electrode for use in micro-electrochemistry. *Electrochem. Commun.* **1999**, *1*, 180−183.

(13) Lill, K. A.; Hassel, A. W. A combined μ-mercury reference electrode/Au counter-electrode system for microelectrochemical applications. *J. Solid State Electrochem.* **2006**, *10*, 941−946.

(14) Hill, J. C.; Choi, K.-S. Effect of Electrolytes on the Selectivity and Stability of n-type WO_3 Photoelectrodes for Use in Solar Water Oxidation. *J. Phys. Chem. C* **2012**, *116*, 7612−7620.

(15) Schultze, J. W.; Lohrengel, M. M. Stability, reactivity and breakdown of passive films. Problems of recent and future research. *Electrochim. Acta* **2000**, *45*, 2499−2513.

(16) Fujii, T.; de Groot, F. M. F.; Sawatzky, G. A. In situ XPS analysis of various iron oxide films grown by NO2-assisited molecular-beam epitaxy. *Phys. Rev. B* **1999**, *59*, 3195−3202.

(17) Morar, J. F.; Himpsel, G.; Hughes, J. L.; McFeely, F. R. High resolution photoemission investigation. The oxidation of W. *J. Vac. Sci. Technol. A* **1985**, *3*, 1477−1480.